Biol Cybern (2014) 108:203–221
DOI 10.1007/s00422-014-0590-x

ORIGINAL PAPER

Biological Cybernetics

A computational model of the effect of gene misexpression on the development of cortical areas

Clare E. Giacomantonio · Geoffrey J. Goodhill

Received: 25 February 2013 / Accepted: 30 December 2013 / Published online: 26 February 2014

Abstract Brain function depends on the specialisation of brain areas. In the murine cerebral cortex, the development of these areas depends on the coordinated expression of several genes in precise spatial patterns in the telencephalon during embryogenesis. Manipulating the expression of these genes during development alters the positions and sizes of cortical areas in the adult. Qualitative data also show that these genes regulate each other's expression during development so that they form a regulatory network with many feedback loops. However, it is currently unknown which regulatory interactions are critical to generating the correct expression patterns to lead to normal cortical development. Here, we formalise the relationships inferred from genetic manipulations into computational models. We simulate many different networks potentially consistent with the experimental data and show that a surprising diversity of networks produce similar results. This demonstrates that existing data cannot uniquely specify the network. We conclude by suggesting experiments necessary to constrain the model and help identify and understand the true structure of this regulatory network.

Keywords Neural development · Embryonic development · Gene regulatory network · Patterning

C. E. Giacomantonio · G. J. Goodhill (✉)
Queensland Brain Institute, The University of Queensland, St Lucia, QLD 4072, Australia
e-mail: g.goodhill@uq.edu.au

C. E. Giacomantonio
e-mail: clareg@gmail.com

G. J. Goodhill
School of Mathematics and Physics, The University of Queensland, St Lucia, QLD 4072, Australia

1 Introduction

The cerebral cortex is divided into functionally specialised areas defined by their cytoarchitecture, connections and gene expression. Whether genes or activity is the principal driver of the development of these specialised areas, a process referred to as arealisation, has been the subject of much debate for many years (Rakic 1988; O'Leary 1989). Evidence has now accumulated that early cortical development is genetically regulated, since altering the expression of some spatially non-uniform genes before innervation from the thalamus alters the positions of cortical areas that emerge postnatally (for reviews, see Sur and Leamey 2001; Grove and Fukuchi-Shimogori 2003; Job and Tan 2003; Sur and Rubenstein 2005; Mallamaci and Stoykova 2006; O'Leary et al. 2007; O'Leary and Sahara 2008; Hébert and Fishell 2008; Rakic et al. 2009; Mallamaci 2011). However, later patterned neuronal activity via thalamocortical inputs also has a role in the refinement of cortical areas, because altering thalamocortical inputs can change area size or respecify area identity (Sur and Leamey 2001; Sur and Rubenstein 2005; Rakic et al. 2009; Mallamaci 2011). Here, we focus on a question concerning the earliest stages of cortical area development: how the spatial patterns of gene expression are created before thalamocortical innervation.

Over the past decade, experiments have identified a 'parts list' of several genes regulating area development that are expressed in gradients across the embryonic mouse brain (O'Leary et al. 2007; Rakic et al. 2009). Manipulating the expression levels of these genes during development alters the emergent anterior-posterior positions of the cortical areas. Moreover, these genes regulate each other's expression during development. However, the vast majority of the data concerning interactions between these genes has come from characterising gene expression patterns by *in situ* hybridisa-

tion in loss-of-function and gain-of-function mice. Accordingly, all data are qualitative, all reasoning verbal rather than mathematical, and which interactions are direct or indirect is largely unknown. The majority of experimental data on the genes involved in arealisation relate five genes that encoding the secreted signalling protein FGF8 and four transcription factors: EMX2, PAX6, COUP-TFI (NR2F1) and SP8. Hence, we focus on these five molecules and use the term gene misexpression experiments to collectively describe observations of the loss-of-function and gain-of-function mice for these five genes.

To date, there has been little computational work directed towards understanding the arealisation regulatory network. Karbowski and Ermentrout (2004) created a broad phenomenological model that incorporated expression gradients of *Fgf8*, *Emx2* and *Pax6*, maintained by assumed interactions. However, they focussed on expression of theoretical downstream guidance cues and a detailed simulation of thalamocortical innervation. Their study was mostly speculative as there are few data available to connect the gradients to guidance cues or constrain models of thalamocortical innervation. In contrast, Giacomantonio and Goodhill (2010) focussed on the early arealisation regulatory network exclusively where experimental data are currently concentrated. Using a Boolean model in which genes can only be active or inactive, they simulated many possible networks potentially consistent with experimental data. This allowed predictions to be made about likely and unlikely interactions in the network based on the probability that a network reached a steady state corresponding to the expression pattern seen in wild-type (WT) mice. However, restriction to only binary levels of gene expression meant that the Boolean model could not make use of the shifted gradient data from gene misexpression mice to provide further constraints.

In contrast, the interplay between experiments and computational modelling of regulatory networks in other systems has been rich and productive. Different types of models have been used according to the quality and type of data available, and the question the model is seeking to answer (Jong 2002). In developmental biology, studies of the regulatory networks controlling segmentation in the *Drosophila* embryo provide an instructive example of how computational and 'wet' experiments can synergise to improve our understanding of a process (Thieffry and Sanchez 2003; Tomlin and Axelrod 2007). Recently, several papers have drawn on earlier work connecting Boolean and continuous representations (Glass and Kauffman 1973) to examine regulatory networks; they use both Boolean models and their transformations into ordinary differential equation (ODE) models, to investigate a richer set of expression dynamics (Wittmann et al. 2009a,b; Nakajima et al. 2010).

In this paper, we formalise the verbal reasoning resulting from experimental data from loss-of-function and gain-of-function mice into a set of ODEs that describe the epistatic relationships between genes. We use the ODE formalism to simulate the dynamics of the five genes and proteins of interest with continuous expression levels. The use of continuous variables allows us to simulate expression patterns under both WT and misexpression conditions and thus use more experimental data to constrain the model than in the Boolean formalism used by Giacomantonio and Goodhill (2010). There have been many misexpression mice created with abnormal cortical area development, but they have been characterised using different methods at different developmental time points. Since we aimed to simulate the dynamics of the gene regulatory network comprised of *Fgf8*, *Emx2*, *Pax*, *Coup-tfi* and *Sp8*, we identified those misexpression mice with published data on the abundance relative to WT of at least one of these transcripts, or the associated proteins, along the anterior-posterior axis. In total, we found eleven misexpression experiments in the literature satisfying these constraints (Fig. 1).

We simulated the dynamics of the many possible networks identified as consistent with WT results by Giacomantonio and Goodhill (2010). In this way, we could still analyse the dynamics of many different possible networks, but eliminate many possibilities. In effect, we used the Boolean model as a heuristic filter to narrow the space of possible networks for further, more computationally intensive investigation. We evaluated the ability of each network to reproduce each of the misexpression experiments in the ODE model using both random sampling and simulated annealing to explore parameter space. We demonstrate that, surprisingly, the performance of networks is not strongly related to their structure. Consequently, we conclude that current experimental data cannot uniquely specify, or even tightly constrain, the true structure of the arealisation regulatory network.

2 Methods

2.1 Networks simulated

In earlier work, Giacomantonio and Goodhill (2010) screened 2^{24} networks potentially consistent with experimental data in a Boolean model. Briefly, each possible network was translated into a set of Boolean logic functions. Repressive interactions became a negation, and the action of multiple regulators on a single gene was combined with a logical conjunction. Functional networks had steady states corresponding to binary versions of the states observed at the anterior and posterior poles of the WT mouse telencephalon at around embryonic day 10.5 (E10.5). Furthermore, when simulated using asynchronous updating, they had a greater than 50 % probability of reaching these steady states when started from the binary versions of the states observed at the anterior

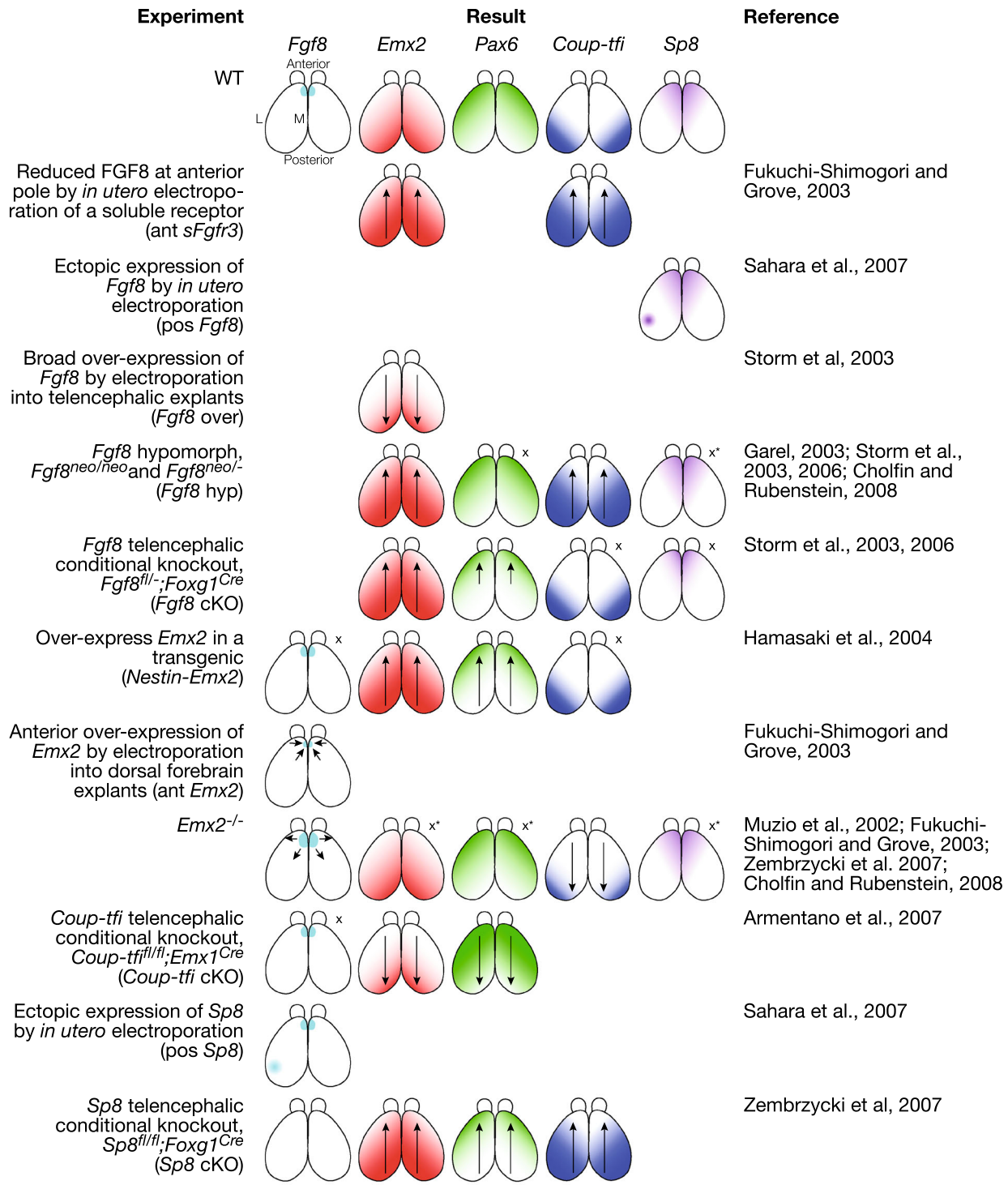

Fig. 1 Schematic of WT expression patterns and the changes in the eleven misexpression experiments simulated in this paper. More detail on each of the misexpression mice is given in the methods, along with how each experiment was translated into model parameters and the criteria we used to classify each simulation steady state as reproducing or not reproducing the experimental data. Arrows indicate the direction in which expression gradients or domains shifted. These results were all reported as qualitative descriptions of changes in sections analysed with *in situ* hybridisation. Hence, there is no clear interpretation of how these gradient profiles changed quantitatively. An 'x' indicates that the expression pattern was indistinguishable from WT. An 'x*' indicates that the minimal interpretation of conflicting or ambiguous results is the presence of a gradient, with no changes relative to WT specified

and posterior poles at around E8. Some additional networks that marginally met these conditions were considered non-functional because they contained combinations of interactions that generally caused networks to have a less than 50 % probability of proceeding reliably from either the anterior starting state to steady state, or the posterior starting state to steady state. In total, the Boolean screen classified 5,849 networks as functional based on WT expression patterns. These are the networks we examined in more detail in this paper. However, for some purposes, we also simulated 5,000 networks randomly chosen from the large pool of non-functional networks in the Boolean model.

2.2 The differential equation model

We examined the dynamics of the networks of interest using a differential equation model. Most of the experimental data on interactions between the genes that regulate cortical area development come from analysis of expression patterns in misexpression mice. Many of these mice exhibit expression gradients that are shifted towards the anterior or posterior poles. These results cannot be reproduced in a two compartment, two level model such as the Boolean model published previously (Giacomantonio and Goodhill 2010). Here, we use a continuous formalism based on ODEs, which is more suited to simulating these experimental data.

We transformed the Boolean models of the networks of interest into ODE models using the procedure outlined by Wittmann et al. (2009a), Wittmann et al. (2009b). There is a normalised continuous variable for each of our species forming the array $X = [x_1, x_2, \ldots x_5, X_1, X_2, \ldots, X_5]$. Here, $[x_1, x_2, \ldots, x_5]$ are variables representing the normalised abundances of the five mRNAs, *Fgf8, Emx2, Pax6, Coup-tfi* and *Sp8*, later denoted $[f, e, p, c, s]$. Similarly, $[X_1, X_2, \ldots, X_5]$ are variables representing the normalised abundances of the five proteins translated from the corresponding mRNAs, later denoted $[F, E, P, C, S]$.

The ODE describing the dynamics of each mRNA, x_i is

$$\frac{d}{dt}x_i(t) = \frac{1}{\tau}\left(\alpha_i \overline{B}_i(X_1(t), X_2(t), \ldots, X_5(t)) + x_{ib} - x_i(t)\right). \tag{1}$$

The right-hand side of this equation consists of several parts: the first two terms describe production of the species x_i, and the final term describes linear decay. The meanings of key variables and parameters are summarised in Table 1.

As the abundances are normalised, we have a single rate for production and decay, described by the lifetime τ (Wittmann et al. 2009b). This could vary between species, but here we fix it to one for all simulations as done previously (Wittmann et al. 2009a).

$\overline{B}_i$ is a continuous homologue of the corresponding Boolean function, B_i. In the transformation, inductive (positive) Boolean step functions were replaced by positive sigmoidal Hill functions, and repressive (negative) Boolean step functions were replaced by negative sigmoidal Hill functions (Dassow et al. 2000; Meir et al. 2002; Wittmann et al. 2009a; Nakajima et al. 2010):

$$\text{inductive} \quad h^+(x_j) = \frac{x_j^n}{x_j^n + k^n} \tag{2}$$

$$\text{repressive} \quad h^-(x_j) = \frac{k^n}{x_j^n + k^n} \tag{3}$$

with free parameters n and k. The actions of multiple regulators were combined with a product

$$\overline{B}_{\text{AND}}(x_i, x_j) = h^{\pm}(x_i) \cdot h^{\pm}(x_j). \tag{4}$$

Two parameters were introduced to Eq. 1 to enable us to simulate misexpression mice. The first is the normalisation constant α_i, which modulates the production term. It normally takes the value one, but is reduced in simulations modelling hypomorphs or knockouts (see section Simulating misexpression mice). The second parameter is the basal

Table 1 Model notation

$[x_1, x_2, x_3, x_4, x_5] = [f, e, p, c, s]$	Variables representing the normalised abundances of mRNAs *Fgf8, Emx2, Pax6, Coup-tfi* and *Sp8*
$[X_1, X_2, X_3, X_4, X_5] = [F, E, P, C, S]$	Variables representing the normalised abundances of proteins FGF8, EMX2, PAX6, COUP-TFI and SP8
τ	The lifetime of species, set to 1
α_i	Normalisation constant for production of mRNA x_i, usually 1 but <1 for some misexpression simulations
β_i	Normalisation constant for production of protein X_i, usually 1 but <1 for some misexpression simulations
x_{ib}	Basal production constant for mRNA x_i, usually 0 but >0 for some misexpression simulations
X_{ib}	Basal production constant for protein X_i, usually 0 but >0 for some misexpression simulations
n	Hill function steepness
k	Hill function threshold

production level x_{ib}. It usually takes the value zero, but is increased in some misexpression simulations to model an additional source of mRNA (again see section Simulating misexpression mice).

The ODE describing the dynamics of each protein X_i is

$$\frac{\mathrm{d}}{\mathrm{d}t}X_i(t) = \frac{1}{\tau}\Big(\beta_i x_i(t) + X_{ib} - X_i\Big). \tag{5}$$

Here, similar to α_i, β_i is normally one but is reduced when the production rate of protein decreases, while X_{ib} is normally zero but is increased when there is an additional protein source (see section Simulating misexpression mice). The linear protein production term (translation) is similar to that used elsewhere (Dassow et al. 2000; Meir et al. 2002; Nakajima et al. 2010).

2.3 Spatial compartments

Since we were interested in anterior-posterior patterning of our genes of interest, the model needed a spatial dimension. This was achieved by introducing two compartments, one anterior and one posterior.

There was no signalling between the compartments. FGF8 is a secreted protein, and there is evidence that it is transported away from its anterior source to form a gradient (Toyoda et al. 2010). Despite this, we did not create more compartments and include FGF8 transport between them because this would offer no additional information. The resulting steady states in the interior compartments would be intermediate between those found at the two poles, and we could not have compared expression profiles to experimental observations using stronger conditions than inequalities since the experimental observations are qualitative.

Since the regulatory network in each compartment was the same, the set of ODEs operating in each compartment was identical. The difference between the two compartments lays in the initial values of the elements of X, denoted $X(0)$. In the WT simulations, all species in the posterior compartment started with zero expression, while in the anterior compartment $x_1(0) = X_1(0) = 1$, but all other species started with zero expression. This was motivated by experimental evidence that *Fgf8* expression at the anterior neural ridge is initiated by genes external to this network, but maintained by this network (O'Leary et al. 2007; Sahara et al. 2007; Zembrzycki et al. 2007). These values were varied in the misexpression simulations as detailed in the next section.

2.4 Simulating misexpression mice

We simulated mRNA and protein dynamics in WT mice, as well as eleven misexpression mice. To simulate each mouse, we varied one or a combination of parameters α_i, β_i, x_{ib} or X_{ib}. This sometimes necessitated a change in $X_i(0)$. In the list below, we summarise each misexpression experiment, the parameter values used to simulate it and the reported expression patterns (see also Fig. 1). There were no additional misexpression datasets that we considered but then discarded because the data were not of sufficient quality.

2.4.1 Reduced FGF8 at anterior pole (ant sFgfr3)

Experiment: Reduce amount of FGF8 at the anterior pole by *in utero* electroporation of a soluble form of one if its receptors, *Fgfr3* at E11.5 (Fukuchi-Shimogori and Grove 2003).

Parameter modifications: $\beta_F^{\mathrm{ant}} = 0.7$, $F^{\mathrm{ant}}(0) = 0.7$.

Result: The *Emx2* and *Coup-tfi* gradients were expanded anteriorly (Fukuchi-Shimogori and Grove 2003).

2.4.2 Ectopic (posterior) expression of *Fgf8* (*pos Fgf8*)

Experiment: Express *Fgf8* ectopically, away from the anterior neural ridge by *in utero* electroporation at E11.5 (Sahara et al. 2007). We simulated this by putting some *Fgf8* in the posterior compartment.

Parameter modifications: $f_b^{\mathrm{pos}} = 0.3$, $f^{\mathrm{pos}}(0) = 0.3$.

Result: Higher than normal expression of *Sp8* in the area of ectopic *Fgf8* (Sahara et al. 2007).

2.4.3 Broad over-expression of *Fgf8* (*Fgf8 over*)

Experiment: Overexpress *Fgf8* broadly by electroporation at E10.5 into telencephalic explants (Storm et al. 2003).

Parameter modifications: $f_b^{\mathrm{ant}} = 0.3$, $f_b^{\mathrm{pos}} = 0.3$, $f^{\mathrm{ant}}(0) = 1.3$, $f^{\mathrm{pos}}(0) = 0.3$. Although the initial anterior abundance of *Fgf8* mRNA is greater than unity, this does not cause runaway production or decay of species regulated by the protein product because the production rates of all targets are limited by the Hill functions to fall in the range (0, 1).

Result: The *Emx2* gradient was compressed posteriorly (Storm et al. 2003).

2.4.4 *Fgf8* hypomorph (*Fgf8 hyp*)

Experiment: This transgenic mouse has been analysed in several papers. They all used a mouse line originally reported in Meyers et al. (1998). In this mouse, the *neo* cassette interferes with *Fgf8* expression, causing aberrant splicing of transcripts. Meyers et al. (1998) reported that *Fgf8* mRNA occurs at less than 45 % of the WT level. We used arealisation data from the homozygous $Fgf8^{\mathrm{neo/neo}}$ mouse reported in Garel et al. (2003) and Cholfin and Rubenstein (2008). We also used data from the heterozygous $Fgf8^{\mathrm{neo/-}}$ mouse created by crossing the heterozygous $Fgf8^{\mathrm{neo/+}}$ mouse with the telencephalic conditional null heterozygote $Fgf8^{+/-}$ (Storm et al. 2003, 2006).

Parameter modifications: $\alpha_f^{\text{ant}} = 0.5$, $\alpha_f^{\text{pos}} = 0.5$, $f^{\text{ant}}(0) = 0.5$, $F^{\text{ant}}(0) = 0.5$.

Result: Both the *Emx2* and *Coup-tfi* gradients expanded anteriorly (Garel et al. 2003; Storm et al. 2003, 2006; Cholfin and Rubenstein 2008). There are conflicting reports on changes to the *Pax6* and *Sp8* gradients. Garel et al. (2003) reported no change in expression of *Pax6* at E14.5 in the $Fgf8^{\text{neo/neo}}$ mouse. Meanwhile, Storm et al. (2006) reported reduced anterior expression at E12.5 in the $Fgf8^{\text{neo/}-}$ mouse. The minimal common result is the presence of a *Pax6* gradient in the same direction as WT. Concerning *Sp8*, Cholfin and Rubenstein (2008) reported no appreciable difference from WT expression at E12.5 in the $Fgf8^{\text{neo/neo}}$ mouse while Storm et al. (2006) reported almost absent expression at E9–9.5 in the $Fgf8^{\text{neo/}-}$ mouse. The minimal common result is higher anterior expression of *Sp8* than posterior.

2.4.5 *Fgf8 telencephalic conditional knockout (Fgf8 cKO)*

Experiment: Delete *Fgf8* in cells that normally express *Foxg1* by Cre-lox recombination (Storm et al. 2003, 2006). These are cells of the anterior neural ridge at around E8 and cells of the whole telencephalic ventricular zone by E9.5 (Hébert and McConnell 2000). In these mice, there is quite a large residual expression of *Fgf8* at E10.5 but it remains confined to the anterior neural ridge (Storm et al. 2003). The level of *Fgf8* mRNA in this mouse is higher than in the *Fgf8* hypomorphs (Storm et al. 2003).

Parameter modifications: $\alpha_f^{\text{ant}} = 0.7$, $\alpha_f^{\text{pos}} = 0.7$, $f^{\text{ant}}(0) = 0.7$, $F^{\text{ant}}(0) = 0.7$.

Result: The *Emx2* gradient was expanded anteriorly (Storm et al. 2003, 2006) while *Pax6* is reported as having reduced anterior expression (Storm et al. 2006). There appears to be little effect on the *Coup-tfi* gradient although decreased brain size makes changes difficult to detect (Storm et al. 2006). The *Sp8* expression domain changed shape slightly, extending expression to encompass the midline, but remained high anteriorly and low posteriorly (Storm et al. 2006).

2.4.6 *Over-express Emx2 in a Nestin–Emx2 transgenic (Nestin–Emx2)*

Experiment: The *Emx2* gene is placed between the *Nestin* promoter and a *Nestin* enhancer to express additional *Emx2* in cells that usually express *Nestin*; these are the progenitors of the cortical ventricular zone from E9.5 (Hamasaki et al. 2004). Northern blot analysis of the homozygote showed transgene levels in the forebrain were 42 ± 2 % (mean $\pm$ standard error of the mean) at E11.5, 39 ± 3 % at E13.5 and 48 ± 2 % at E15.5.

Parameter modifications: $e_b^{\text{ant}} = 0.3$, $e_b^{\text{pos}} = 0.3$, $e^{\text{ant}}(0) = 0.3$, $e^{\text{pos}}(0) = 0.3$, $E^{\text{ant}}(0) = 0.3$, $E^{\text{pos}}(0) = 0.3$.

Result: Expression of *Fgf8* and *Coup-tfi* was unchanged (Hamasaki et al. 2004). Expression of *Emx2* increased relative to WT from E9.5–E12.5, while *Pax6* expression decreased (Hamasaki et al. 2004).

2.4.7 *Anterior over-expression of Emx2 (ant Emx2)*

Experiment: Over-express *Emx2* at the anterior pole of whole dorsal forebrain explants at E10.5 by electroporation (Fukuchi-Shimogori and Grove 2003).

Parameter modifications: $e_b^{\text{ant}} = 0.3$, $e^{\text{ant}}(0) = 0.3$.

Result: Decreased *Fgf8* expression at anterior neural ridge (Fukuchi-Shimogori and Grove 2003).

2.4.8 *Emx2*$^{-/-}$

Experiment: The $Emx2^{-/-}$ mouse produces non-functional EMX2 protein (Pellegrini et al. 1996). We used arealisation data from this mouse reported in Muzio et al. (2002), Fukuchi-Shimogori and Grove (2003), Zembrzycki et al. (2007) and Cholfin and Rubenstein (2008).

Parameter modifications: $\beta_E^{\text{ant}} = 0$, $\beta_E^{\text{pos}} = 0$.

Result: The *Fgf8* domain was expanded (Fukuchi-Shimogori and Grove 2003; Cholfin and Rubenstein 2008) and more intense (Cholfin and Rubenstein 2008). Muzio et al. (2002) report that the *Emx2* gradient was compressed while the *Pax6* gradient was expanded along the medial-lateral axis, based on coronal sections. Since they did not report expression along the anterior-posterior axis, we only assumed the presence of an anterior-posterior gradient in the same direction as WT. The *Coup-tfi* gradient was compressed (Cholfin and Rubenstein 2008). *Sp8* expression is variously reported as expanded posteriorly (Cholfin and Rubenstein 2008) and unchanged or reduced (Zembrzycki et al. 2007). The minimal common result is the presence of a *Sp8* gradient in the same direction as WT.

2.4.9 *Coup–tfi telencephalic conditional knockout (Coup–tfi cKO)*

Experiment: Delete *Coup-tfi* in cells that normally express *Emx1* by Cre-lox recombination (Armentano et al. 2007). These are cells of the cortical ventricular zone from around E10.5 (Gorski et al. 2002), coincident with when *Coup-tfi* expression commences (Armentano et al. 2007).

Parameter modifications: $\alpha_c^{\text{ant}} = 0$, $\alpha_c^{\text{pos}} = 0$.

Result: Expression of *Fgf8* was unchanged, while the *Emx2* gradient was compressed posteriorly and the *Pax6* gradient was expanded posteriorly (Armentano et al. 2007).

2.4.10 Ectopic (posterior) expression of Sp8 (pos Sp8)

Experiment: Express *Sp8* ectopically by *in utero* electroporation at E11.5 (Sahara et al. 2007). We simulated this by putting some *Sp8* in the posterior compartment.

Parameter modifications: $s_b^{\text{pos}} = 0.3$, $s^{\text{pos}}(0) = 0.3$.

Result: Ectopic expression of *Fgf8* in the area of ectopic *Sp8* (Sahara et al. 2007).

2.4.11 Sp8 telencephalic conditional knockout (Sp8 cKO)

Experiment: Delete *Sp8* in cells that normally expression *Foxg1* by Cre-lox recombination (Zembrzycki et al. 2007). These are cells of the anterior neural ridge at around E8, and cells of the whole telencephalic ventricular zone by E9.5 (Hébert and McConnell 2000), coincident with the usual spatio-temporal expression of *Sp8* (Zembrzycki et al. 2007).

Parameter modifications: $\alpha_s^{\text{ant}} = 0$, $\alpha_s^{\text{pos}} = 0$.

Result: Zembrzycki et al. (2007) report that *Fgf8* expression at the anterior neural ridge was unchanged at E9.5, but lost at the midline at E12.5. We interpret these observations into a requirement that *Fgf8* expression is minimally expressed at steady state. Meanwhile, the *Emx2* and *Coup-tfi* gradients were expanded anteriorly and the *Pax6* gradient compressed anteriorly (Zembrzycki et al. 2007).

2.5 Parameter search

The ODE formalism introduced several free parameters but we were primarily interested in the effect of the Hill steepness n and threshold k, which are critical to the dynamics of the ODEs describing mRNA abundance (Eq. 1).

2.5.1 Random sampling

In our first set of simulations, we sampled n and k values randomly and independently for each interaction, as done previously (Dassow et al. 2000). In an effort to adequately sample different regions of parameter space but still examine the dynamics of the 5,849 networks of interest in reasonable computational time, we drew n from a limited set of three possible values $\{1, 2, 8\}$ and k from the limited set $\{0.2, 0.5, 0.8\}$. We performed 10^5 random samples from these sets for each network.

2.5.2 Simulated annealing

In the simulated annealing optimisations, the objective function was the number of experiments reproduced, $N(\mathbf{n}, \mathbf{k})$ where $\mathbf{n}$ and $\mathbf{k}$ are vectors of the Hill parameters for each interaction. We used this function even though it is discontinuous because it is simple and intuitively meaningful. The Hill coefficients $\mathbf{n}$ were restricted to the range $[1, 8]$ while the Hill thresholds $\mathbf{k}$ were restricted to the range $[0, 1]$. Each search was started at a random point in parameter space. At each iteration, a step was taken from the current point in parameter space $(\mathbf{n}, \mathbf{k})$ to a point nearby $(\mathbf{n}', \mathbf{k}')$. The size and sign of the step were chosen randomly with a maximum size of 5 % of the width of the range of that variable. If the performance of the network increased, then the new parameter values were accepted. If the performance decreased, then the parameter values were accepted with probability $P(T) = exp(-(N(\mathbf{n}', \mathbf{k}') - N(\mathbf{n}, \mathbf{k}))/T)$ where T is the temperature. The temperature started at 1 and was decreased after either 1,000 moves were attempted or 100 moves accepted. Temperature was decreased at a rate of 0.99, and the search was terminated when $T < 0.1$.

2.5.3 Genetic algorithm

In the genetic algorithm optimisations, we used the same objective function as for simulated annealing. We chose a real-valued encoding to represent each chromosome so that the Hill coefficients we were optimising formed a vector of real numbers. Each parameter was restricted to the same bounds as for simulated annealing, and the initial population was chosen randomly. At each generation, we carried the two best parents through to the next generation unchanged. 80 % of the next generation was formed via crossover and the remainder by pure mutation. The chromosome of each of the children formed by crossover was mutated by resetting parameters from a uniform random distribution within the relevant bounds at the mutation rate. Each optimisation was continued for 100 generations. Different combinations of population size, fitness scaling, crossover method and mutation rate were trialled for the best performing network from simulated annealing (that shown in Fig. 3a).

2.6 Simulations

The set of ODEs for each network at each point in parameter space was solved numerically using Matlab (www.mathworks.com). Simulations were terminated when the maximum difference between levels of all species at successive specified time points was less than 0.1 %.

The simulations performed in the study were extensive. We used a computational cluster of approximately 400 2.93GHz processors. The simulations of the 5,849 functional networks from the Boolean model with 10^5 randomly sampled values of n and k took approximately 7 days for WT and a further 35 days for the eleven misexpression experiments. Similar simulations of 5,000 non-functional networks from the Boolean model took approximately 12 days in total. Finally, the single sweep of parameter space using simulated annealing for the 5,849 functional networks

took approximately 120 days, and this lengthy simulation time is the reason why we did not do multiple runs for each network.

2.7 Evaluating whether steady states reproduced experimental data

As stated previously, the experimental data we were attempting to reproduce with this model were anterior-posterior expression gradients. Most misexpression mice exhibit anterior or posterior shifts in these gradients, as shown by *in situ* hybridisation. There are almost no quantitative data on expression levels available for any of these experiments. Hence, the criteria we used to score simulations as matching experiments were inequalities of anterior levels relative to posterior levels (to evaluate gradient direction) and levels relative to WT (to evaluate a shift in gradient).

We could not infer from published data whether shifts in expression gradients corresponded to shallower (steeper) gradients with levels at one end fixed, as could occur if expression at one pole was already at its minimal (maximal) level, or decreased (increased) expression over the whole telencephalon. For example, the *Emx2* gradient is normally low anteriorly and high posteriorly (Fig. 2a, blue line). The posterior shift in this gradient described in the *Coup-tfi* cKO (Armentano et al. 2007) could correspond to a shallower gradient (Fig. 2a, red line), or a constant absolute decrease in *Emx2* across the whole telencephalon (Fig. 2a, green line). If the minimum possible expression of *Emx2* was '2', then instead a uniform absolute decrease, the lower limit would be thresholded (Fig. 2a, yellow line). Given the uncertainty in the shape of gradients, we used the minimal interpretation that when a gradient is compressed, expression in the high concentration compartment must decrease relative to WT, while expression in the low concentration compartment could be less than or equal to the WT level. Similarly, for gradient expansion, expression in the low concentration compartment had to increase relative to WT, while expression in the high concentration compartment could be greater than or equal to WT.

The inequalities used to evaluate matches to each experiment can be found in Table 2. These are derived from the experimental results summarised after our description of each misexpression mouse in Sect. 2.4 and in Fig. 1.

As they appear in Table 2, the inequalities could be satisfied by very small differences in abundance between the two compartments or between WT and a misexpression simulation. Since we know that the changes *in vivo* are large enough to be detected with non-quantitative methods, we investigated the effect of minimum thresholds for change detection. We investigated the imposition of a spatial gradient detection threshold and an abundance change detection threshold separately, but we present the results of changing them simultaneously since this illustrates our findings adequately. We ultimately settled on using a value of 0.1 for both thresholds.

2.8 Structural metrics

We calculated in the undirected degree, indegree, outdegree, total degree (indegree + outdegree) and directed clustering coefficient of each node, considering a gene and its associated protein as a single entity. A description of the undirected degree, indegree, outdegree and total degree and undirected degree is given with the results. The directed clustering coefficient of each gene/protein pair was calculated using the algorithm from Fagiolo (2007), implemented by Gleich (2009). We then calculated the Pearson's and Spearman's correlation coefficient between the mean, minimum and maximum of each metric for each network and the maximum number of experiments reproduced by that network by any method. We also calculated the correlation between performance and the number of repressive interactions and reciprocal repressive loops in each network.

3 Results

3.1 Networks simulated using differential equation models

We aimed to reproduce the gene expression patterns in WT as well as eleven misexpression mice. Most of the constraints for the model came from the misexpression experiments, but we began by examining WT dynamics because changes in the misexpression experiments are defined relative to WT, so a simulation was only scored as fulfilling the criteria for reproducing a misexpression experiment if it also fulfilled the WT matching criteria.

We began by simulating 5,849 different networks comprised of the genes and proteins of interest. These were the functional networks identified by simulations of WT dynamics in Boolean models (Giacomantonio and Goodhill 2010 and see methods for further detail). We transformed the Boolean model of each network into an ODE model using the procedure outlined by Wittmann et al. (2009a), Wittmann et al. (2009b). The action of each protein regulator on a target gene took the form of a sigmoidal Hill function (see methods). This introduced two free parameters for each interaction, a steepness n and threshold k. All steady states in the Boolean models are also steady states in the ODE models, for appropriate values of n and k (Wittmann et al. 2009b), but for other values of n and k, there may be additional steady states in the ODE models. Hence, we examined network dynamics for different values of n and k. We explored

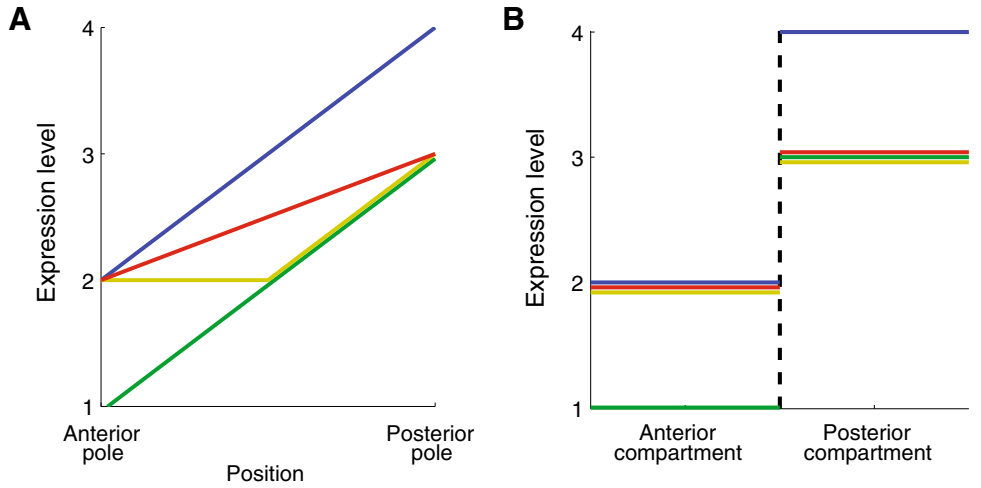

Fig. 2 The representation of gradients and their misexpression in the model. **a** The wild-type gradient is represented by a *blue line* (the expression levels 1–4 are arbitrary and for illustration purposes only). The description of this gradient as being shifted posteriorly or down-regulated in a misexpression mouse (e.g. the *Emx2* gradient in the *Coup-tfi* cKO Armentano et al. 2007) could correspond to a number of possibilities in the real data, shown by the *red*, *yellow* and *green lines*. *Red* shows a uniformly shallower gradient, while *green* shows a uniform absolute decrease. If the minimum possible expression of this particular species is '2', then there is a minimum threshold and the posterior shift might take the form of the *yellow line*. **b** In our model, we have two compartments, one corresponding to the anterior pole and the other to the posterior pole. This panel depicts the levels in these two compartments corresponding to the different cases in *A*. As we do not know which case occurs in real misexpression experiment, we evaluate model output using the criteria that the misexpressed anterior level should be less than or equal to the WT anterior level, and that the misexpressed posterior level should be less than the WT posterior level (color figure online)

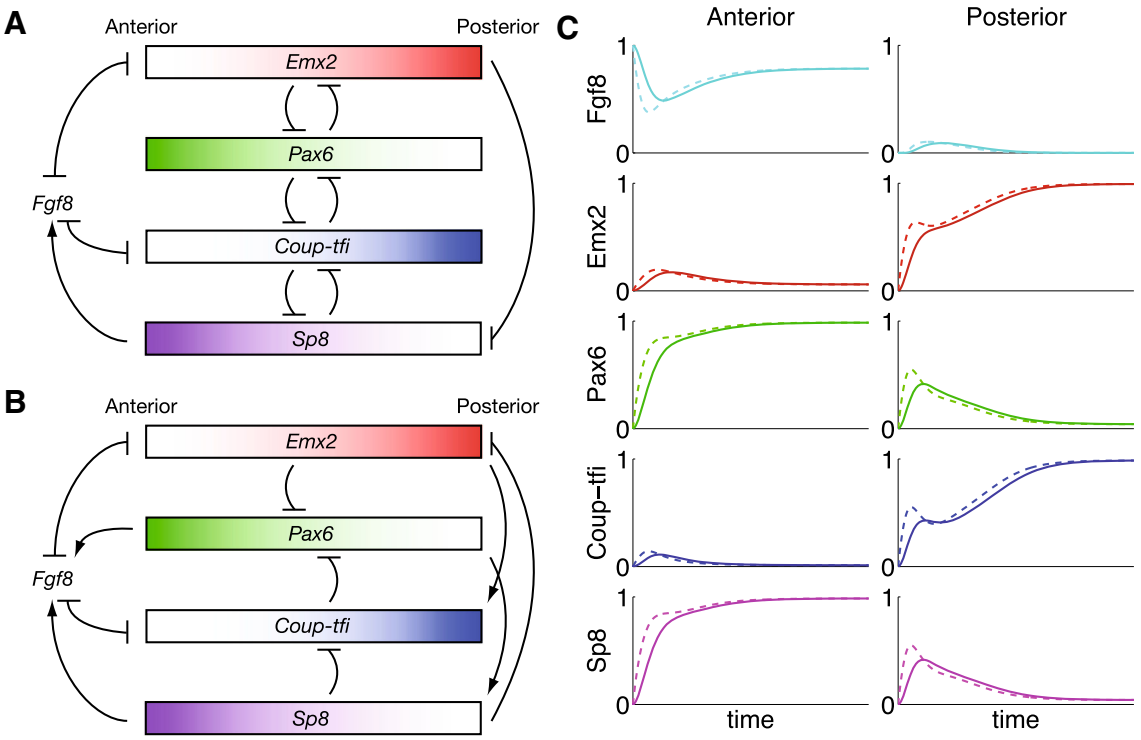

Fig. 3 Two example networks and an example WT simulation. **a** The network which was able to reproduce the most experimental data. **b** A network with a quite different structure to the best performing network, but a similar level of performance. In these networks, each gene generates its associated protein, and the lines between genes indicate how the protein products influence other genes. *Arrows* indicate inductive interactions *while flat-headed lines* indicate repressive interactions. **c** Example WT simulation of the network in **a** for $n = 2$ and $k = 0.5$ for all interactions. Note that the system reaches a steady state that matches the relative expression levels observed at the anterior and posterior poles. The *dashed lines* are mRNA abundance, and solid lines are protein abundance

Table 2 Criteria used to evaluate whether the steady states of models matched experimental observations

Experiment	f	F	e	E	p	P	c	C	s	S
WT	$f_{ant} > f_{pos}$	$F_{ant} > F_{pos}$	$e_{ant} < e_{pos}$	$E_{ant} < E_{pos}$	$p_{ant} > p_{pos}$	$P_{ant} > P_{pos}$	$c_{ant} < c_{pos}$	$C_{ant} < C_{pos}$	$s_{ant} > s_{pos}$	$S_{ant} > S_{pos}$
ant *sFgfr3*	–	–	$e_{ant} < e_{pos}$ $e_{ant} > e_{ant}^{WT}$ $e_{pos} \geq e_{pos}^{WT}$	–	–	–	$c_{ant} < c_{pos}$ $c_{ant} > c_{ant}^{WT}$ $c_{pos} \geq c_{pos}^{WT}$	–	–	–
pos *Fgf8*	–	–	–	–	–	–	–	–	$s_{pos} > s_{pos}^{WT}$	–
Fgf8 over	–	–	$e_{ant} < e_{pos}$ $e_{pos} < e_{pos}^{WT}$ $e_{ant} \leq e_{ant}^{WT}$	–	–	–	–	–	–	–
Fgf8 hyp	–	–	$e_{ant} < e_{pos}$ $e_{ant} > e_{ant}^{WT}$ $e_{pos} \geq e_{pos}^{WT}$	–	$p_{ant} > p_{pos}$	–	$c_{ant} < c_{pos}$ $c_{ant} > c_{ant}^{WT}$ $c_{pos} \geq c_{pos}^{WT}$	–	$s_{ant} < s_{pos}$	–
Fgf8 cKO	–	–	$e_{ant} < e_{pos}$ $e_{ant} > e_{ant}^{WT}$ $e_{pos} \geq e_{pos}^{WT}$	–	$p_{ant} > p_{pos}$ $p_{ant} < p_{ant}^{WT}$	–	$c_{ant} < c_{pos}$	–	$s_{ant} < s_{pos}$	–
Nestin-Emx2	$f_{ant} > f_{pos}$	–	$e_{ant} < e_{pos}$ $e_{ant} > e_{ant}^{WT}$ $e_{pos} \geq e_{pos}^{WT}$	–	$p_{ant} > p_{pos}$ $p_{ant} < p_{ant}^{WT}$ $p_{pos} \leq p_{pos}^{WT}$	–	$c_{ant} < c_{pos}$	–	–	–
ant *Emx2*	$f_{ant} > f_{pos}$ $f_{ant} < f_{ant}^{WT}$ $f_{pos} \leq f_{pos}^{WT}$	–	–	–	–	–	–	–	–	–
$Emx2^{-/-}$	$f_{ant} > f_{pos}$ $f_{pos} > f_{pos}^{WT}$ $f_{ant} \geq f_{ant}^{WT}$	–	$e_{ant} < e_{pos}$	–	$p_{ant} > p_{pos}$	–	$c_{ant} < c_{pos}$ $c_{pos} < c_{pos}^{WT}$ $c_{ant} \leq c_{ant}^{WT}$	–	$s_{ant} < s_{pos}$	–
Coup-tfi cKO	$f_{ant} > f_{pos}$	–	$e_{ant} < e_{pos}$ $e_{pos} < e_{pos}^{WT}$ $e_{ant} \leq e_{ant}^{WT}$	–	$p_{ant} > p_{pos}$ $p_{pos} > p_{pos}^{WT}$ $p_{ant} \geq p_{ant}^{WT}$	–	–	–	–	–
pos *Sp8*	$f_{pos} > f_{pos}^{WT}$	–	–	–	–	–	–	–	–	–
Sp8 cKO	$f_{ant} = 0$ $f_{pos} = 0$	–	$e_{ant} < e_{pos}$ $e_{ant} > e_{ant}^{WT}$ $e_{pos} \geq e_{pos}^{WT}$	–	$p_{ant} > p_{pos}$ $p_{ant} < p_{ant}^{WT}$ $p_{pos} \leq p_{pos}^{WT}$	–	$c_{ant} < c_{pos}$ $c_{ant} > c_{ant}^{WT}$ $c_{pos} \geq c_{pos}^{WT}$	–	–	–

In evaluating each of the inequalities we imposed detection threshold of 10 %

n and k parameter space using two different methods, of increasing computational complexity: random sampling and then simulated annealing to re-examine the best performing networks.

3.2 WT dynamics

Initially, we sampled n and k randomly for each interaction from a limited set of nine possible combinations. Our 5,849 networks of interest have between 5 and 15 interactions each, with a mean of 9.7, giving between 9^5 and 9^{15} (mean $9^{9.7} \approx 10^9$) possible simulations if the n and k combinations were sampled exhaustively. We performed only 10^5 random samples due to computational limitations (see methods), giving limited coverage of parameter space in most cases.

Our initial simulations of WT networks with this simple sampling method showed that these networks can robustly reproduce the WT expression patterns observed experimentally, while networks previously excluded by the Boolean analysis cannot. An example time course of mRNA and protein abundance for a particular set of n and k values is shown in Fig. 3c for the network in Fig. 3a. When evaluating the steady states, we scored matches to WT using the criteria in Table 2 with a 10 % detection threshold (see methods for further detail). Imposing a threshold reduced the number of simulations that scored as matching WT, but as the threshold increased, the reduction quickly plateaued (Fig. 4a). Even with limited sampling of the Hill steepness and threshold, 22.7 % of all simulations reached the WT steady state with a detection threshold of 10 %. For each network, between 4.9 and 47.2 % of combinations were scored as matching WT (Figs. 4a and 5, WT). Thus, for these networks, it was easy to find regions of parameter space, which reproduced the WT expression gradients.

In contrast, similar simulations of 5,000 networks drawn randomly from the large pool of non-functional networks identified in the Boolean model did not robustly reproduce the WT expression patterns observed experimentally. Only 0.2 % of all simulations were scored as matching WT with a 10 % steepness threshold (Fig. 4b). At this threshold, 97.9 % of networks did not reach WT steady state for any combination of n and k, and the mean number of combinations scored as matching WT was 204 out of 10^5 (0.2 %) (Fig. 5, WT). Thus, most non-functional networks from the Boolean analysis did not reproduce the WT gradients in the ODE model either, and the few that did reproduce the WT gradients generally did so in a small region of parameter space. Hence, while the Boolean analysis is not a perfect filter, it is a reasonable and therefore useful heuristic for narrowing the space of networks for further analysis in the more realistic, ODE model.

3.3 Simulations of misexpression experiments for possible arealisation networks

For each combination of n and k that was scored as a WT match in each network, we modified model parameters as described in methods to simulate the eleven misexpression experiments summarised in Fig. 1. Using random sampling, we found that some simulation steady states reproduced the changes in expression patterns seen in each of the misexpression experiments (Fig. 5, solid lines). Similar simulations of misexpression experiments for the non-functional networks from the Boolean analysis produced many times fewer matches to each of the misexpression mice for all combinations of Hill parameters trialled (Fig. 5, dashed lines).

We were interested to see whether it was possible to identify networks that were consistent with both WT gradients and the changes seen in the eleven misexpression experiments, in a single region of Hill steepness and threshold parameter space. None of the networks we simulated could do this for the combinations of Hill steepness and threshold we trialled (Fig. 6a). At best, two networks reproduced the WT expression gradients as well as the changes in eight out of eleven misexpression mice. Of the 5,000 non-functional network from the Boolean model, at best twelve networks reproduce WT and the changes in seven out of eleven misexpression mice (Fig. 6b). Although this performance is not much worse than the functional Boolean networks, these few networks were atypical of the performance of the non-functional networks (Fig. 6b). To explore parameter space further for the functional networks, we used simulated annealing (Kirkpatrick et al. 1983) and genetic algorithms (Holland 1975), which have both been shown to be effective at finding regions of parameter space that display a desired behaviour in models with large numbers of free parameters (Vanier and Bower 1999).

A single sweep of parameter space with simulated annealing improved the best performance of many networks. For 71 % of these networks, performance improved with simulated annealing relative to random sampling. Now, at best, one network reproduced the WT expression gradients as well as the changes in ten out of eleven misexpression experiments (all except *Coup-tfi* cKO) (Fig. 6c). This is the network shown in Fig. 3a. We performed ten additional parameter space searches with simulated annealing for this network, but did not find any region of parameter space with better performance. A further 72 networks reproduced WT and nine misexpression experiments, but notably not the same nine. Hence, different sets of misexpression experiments are reproduced by different networks, and it is not the case that this group of networks as a whole consistently reproduces a specific subset of experiments to the mutual exclusion of other experiments.

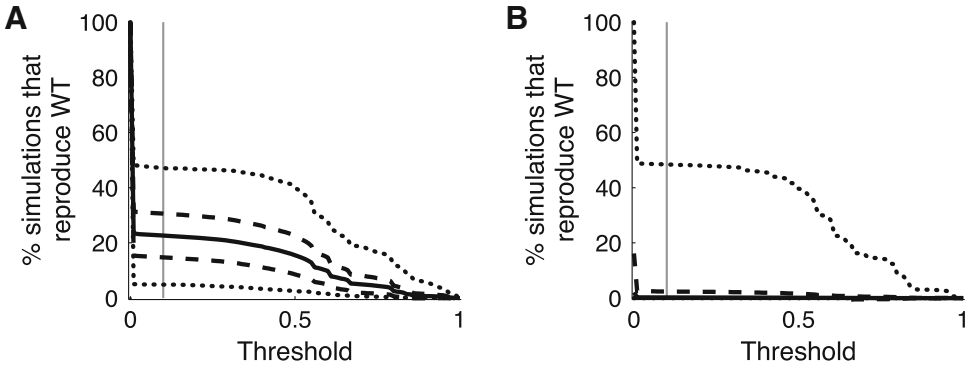

Fig. 4 Effect of thresholding. Percentage of all simulations with random parameter sampling that reproduce WT at various thresholds for detecting a gradient. **a** Simulations of the 5,849 functional networks from the Boolean model. Each network was simulated with 10^5 randomly sampled combinations of n and k. The *solid black line* shows the mean proportion of simulations that reproduced the WT gradients at each threshold across all networks. The *dashed lines* indicate ± one standard deviation, and the *dotted lines* indicate the minimum and maximum over networks. The *vertical grey line* indicates the 10 % steepness threshold that was used for the remaining analysis. **b** Simulations of 5,000 randomly chosen non-functional networks in Boolean model. Note that the *solid black line* indicating the mean proportion of simulations that reproduced the WT gradients lies almost along 0 %

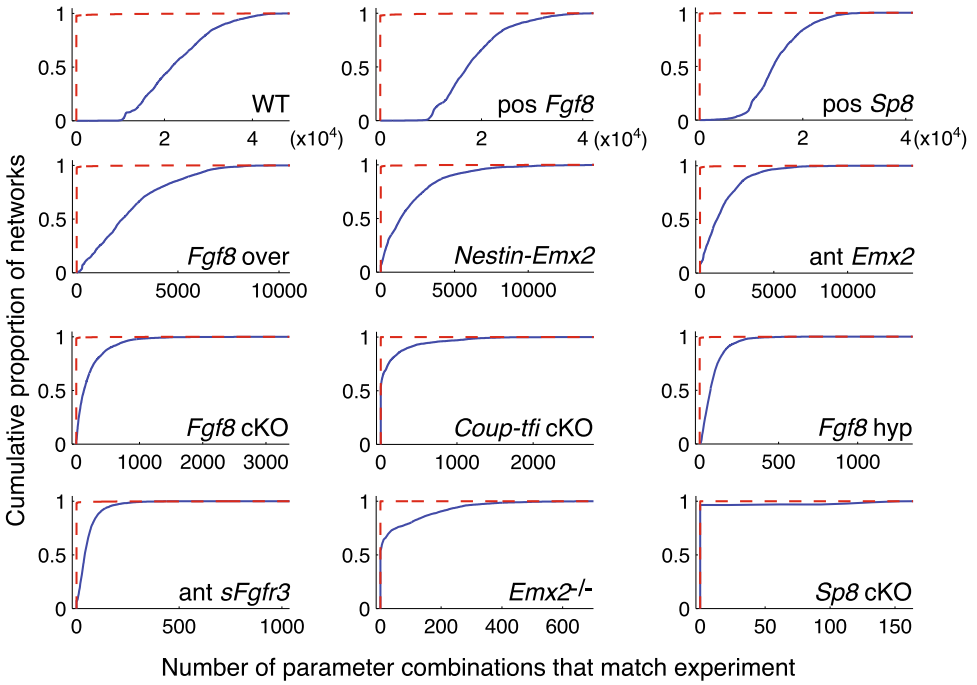

Fig. 5 The cumulative distributions of the proportion of randomly sampled n and k combinations for which simulation steady states matched experiments. Each network was simulated with 10^5 randomly sampled combinations of n and k. Note that the scaling of the x-axis changes between panels. The *blue, solid lines* show the cumulative distributions over the 5,849 functional networks from the Boolean model. The changes seen in each misexpression experiment were reproduced by at least one functional network for one combination of n and k. For many networks, there were many combinations of n- and k-values where steady states matched experimental observations. The *red*, *dashed lines* show the cumulative distributions over 5,000 randomly chosen non-functional Boolean networks. In contrast to the functional networks, in general, the simulation steady states for these networks did not reproduce experimental observations for many of the combinations of n and k investigated indicating that in general, the non-functional networks from the Boolean analysis were also non-functional in the ODE model (colour figure online)

Although we did not identify any networks that could reproduce WT and all eleven misexpression experiments in a single region of parameter space, we suggest that such a region is nevertheless likely to exist for many of the networks we examined. With between 10 and 30 free Hill parameters in each network, our sampling of the vast parameter space is necessarily limited. Given this fact, the performance achieved by many networks is remarkable, and hence, it seems likely

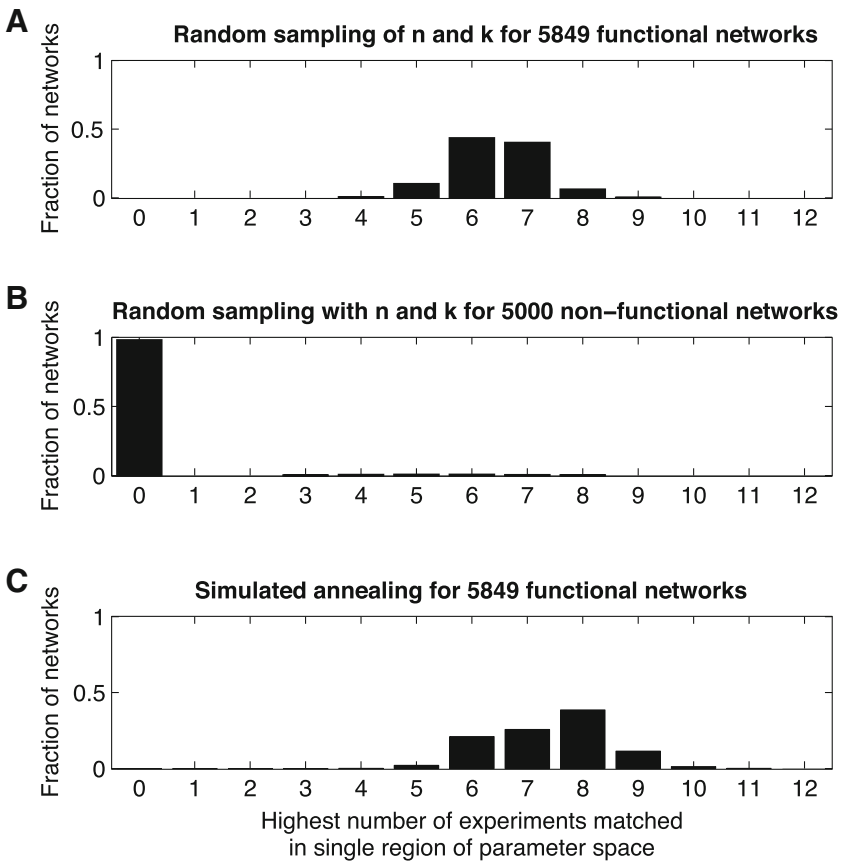

Fig. 6 Performance of networks under random Hill parameter sampling and simulated annealing. Performance is measured as the highest number of experiments that could be reproduced for a single set of Hill parameters, for that Hill parameter sampling method. **a** With random sampling, the 5,849 functional networks reproduce a maximum of 9 experiments and a mean of 6.4 experiments. **b** With random sampling, the 5,000 randomly chosen non-functional networks reproduce a maximum of 8 experiments and a mean of 0.1. **c** Under simulated annealing, 71 % of networks (4,124 networks out of 5,849) have improved performance compared to random sampling, while 6 % (377) have poorer performance and 23 % (1,348) have equal performance

that a region or regions of parameter space exist where WT and all eleven misexpression experiments can be reproduced.

The 'valid' volume of parameter space in which a particular network can reproduce a particular experiment and the valid range of each parameter can be estimated from the simulations with random sampling. For example, for the network in Fig. 3a, 32.9 % of parameter combinations generated expression patterns that matched WT from 10^5 random choices of n and k. The valid volumes for the misexpression experiments were between 0.05 and 24.3 %. From these volumes, we can calculate the chance that a random choice of n and k for an individual interaction lies in a valid volume (Dassow et al. 2000). The network has Fig. 3a has 12 interactions, giving a 24-dimensional Hill parameter space to search. This gives an estimated 95.5 % chance that a random choice of n and k for any individual interaction will be compatible with the WT expression patterns ($0.955^{24} \approx 32.9$ %). Similar calculations for reproducing each of the misexpression experiments for this network indicate chances of an individual Hill parameter being valid between 72.8 and 94.3 %. These valid ranges are large enough that it is reasonable to expect that there is some region of parameter space where all valid ranges overlap for all parameters across experiments (as long as particular sets of experiments are not mutually exclusive). However, the vastness of parameter space makes these regions difficult to find.

The valid volumes for each of the misexpression experiments are not independent, but we found no obvious sets of experiments that are mutually exclusive. In the simulations of the network in Fig. 3a with random sampling, several combinations of experiments were never simultaneously reproduced, but with simulated annealing, we found a region of parameter space where these same experiments were all simultaneously reproduced, and a different experiment excluded. Hence, sets of experiments do not appear to be mutually exclusive for this network, and our failure to find a region of parameter space where the valid volumes for all experiments overlap is likely primarily due to the size of parameter space. However, we cannot exclude the possibility that the data we have modelled are itself not self-consistent. An additional difficulty could be created by the shape of parameter space (Meir et al. 2002; Chaves et al. 2008; Dayarian et al. 2009); if the valid volumes are not continuous, this would make identifying overlapping volumes by simulated annealing particularly difficult.

We therefore also examined the performance of a genetic algorithm in searching this parameter space by performing several optimisations for the network in Fig. 3a. We explored

a few different algorithm choices, as described in the methods. At best, the genetic algorithm found a region of parameter space where the network reproduced the WT expression patterns as well as changes in five out of eleven misexpression mice (data not shown). This is a worse performance than that achieved with simulated annealing (WT and ten misexpression mice) or even large-scale random sampling (WT and six misexpression mice). (Note though that we expect the performance using the genetic algorithm to be as good or better than that of random sampling as the number of runs or the population increases.) Since simulated annealing gave better performance, we did not explore the use of genetic algorithms further on other networks.

3.4 Network performance is only weakly related to structure

Since many networks reproduced most of the existing experimental data, we looked for relationships between various network structure metrics and performance. For each gene/protein pair in each network, we calculated the undirected degree (total number of connections going in or out of the gene or protein, ignoring the direction of the connections), indegree (number of regulators of the gene), outdegree (number of targets of the protein), total degree (total number of regulators of the gene plus targets of the protein) and directed graph clustering coefficient (Fagiolo 2007). Since these metrics are calculated for each gene/protein pair, there was a distribution of each metric for each network. We determined the linear (Pearson's) and rank (Spearman's) correlation between the mean (Fig. 7a), minimum (Fig. 7b) and maximum (Fig. 7c) of these distributions and network performance. In addition, we examined the correlation between performance and the number of repressive interactions, as well as the number of reciprocal repressive loops (Fig. 7d, e), since these are prominent in the structure of the best performing network (Fig. 3a) and have been emphasised in the literature (Mallamaci and Stoykova 2006; O'Leary et al. 2007; Hébert and Fishell 2008).

Many metrics have weak but significant positive correlation with performance (Fig. 7). In general, networks with higher connectivity reproduced more experimental data; however, the correlation is weak. The strongest correlation with network performance occurs for the number of repressive interactions and reciprocal repressive loops in a network, but knowledge of these metrics for any individual network is still a poor predictor of performance. Hence, we conclude that the number of misexpression experiments that each network can reproduce is not strongly determined by these structural statistics, and that a diversity of networks performs similarly.

To illustrate this point further, we present in more detail the performance of the network shown in Fig. 3b, which has quite a different structure to the best performing network in Fig. 3a, but a similar performance. This network includes four interactions not present in the best performing network and is missing four interactions that are present in the best performing network. Figure 3a contains eleven repressive interactions and five reciprocal repressive loops while Fig. 3b contains eight repressive interactions and two reciprocal repressive loops. To enable a fair comparison of performance, we executed ten additional searches of parameter space for network 3B with simulated annealing, as we already did for the best performing network. Despite the structural differences, this network reproduced WT as well as nine out of the eleven misexpression experiments, only one experiment short of the performance of the best network, illustrating that networks with diverse structures perform similarly.

4 Discussion

We have presented a differential equation model of the control of gene expression in WT and several gene misexpression mice by a gene regulatory network. After evaluating the plausibility of different networks by matching the model outputs with current qualitative experimental data, we conclude that many simple networks of five genes can reproduce most of these data, with few requirements on connectivity.

The most important conclusion to draw from these results is that the structure of this network is currently far from being understood, and is likely to be under constrained by current experimental data. Thus, while it is tempting to summarise experimental data in network diagrams similar to those seen in Fig. 3a, b, there are, in fact, many such diagrams consistent with the data. While useful as a summary, our analysis demonstrates that these diagrams have limited utility as conceptual models, and the data principally provide a parts list, not a network structure. Our finding that a diversity of network structures reproduces almost all current data equally well demonstrates that current data are insufficient to uniquely specify the true arealisation network.

Future research on this network may reveal that the arealisation network in WT mice is in fact robust to large perturbations in interaction strengths and even structure, and this property could be of biological relevance. Given the limitations of our modelling to date, and the paucity of data, it is difficult to speculate too much in this direction. However, using a regulatory network to pattern the developing telencephalon with gradients could give a balance between robustness and adaptability that could be an important mechanism in the evolutionary divergence in the relative sizes of cortical areas across mammals. The intriguing possibility that variation in kinetic parameters and initial conditions could be a mechanism for evolution is supported by evidence from

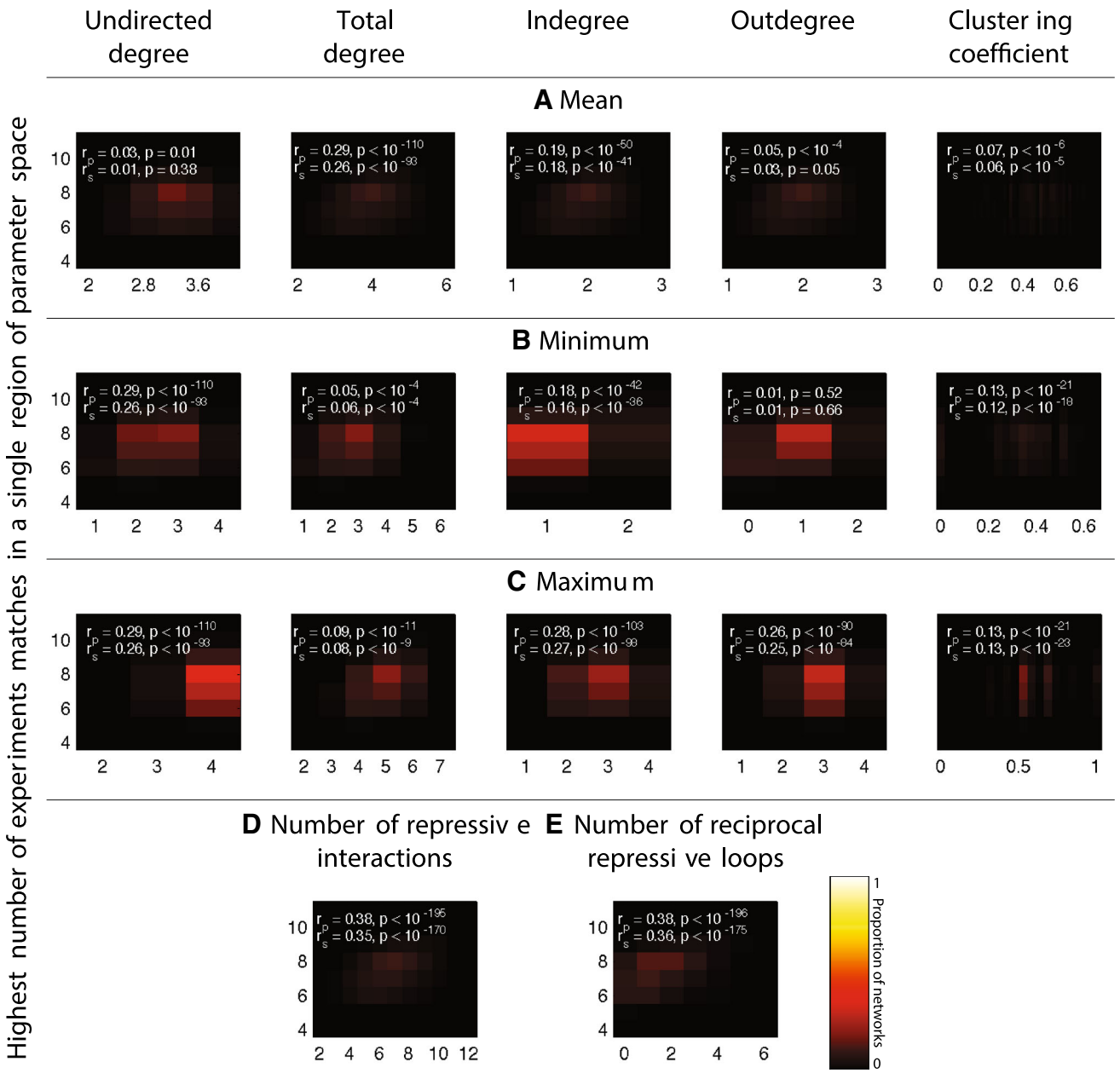

Fig. 7 Performance of networks is not strongly related to their structure. **a–c** The five columns are connectivity metrics that are calculated per gene, giving a distribution for each network. The correlation of performance with the mean (**a**), minimum (**b**) and maximum (**c**) of these distributions is shown in *first three rows*. **d** The correlation between the number of repressive interactions in a network and performance. **e** The correlation between the number of reciprocal repressive loops and performance. A description of the metrics is given in the main text. In all cases, performance is measured as the highest number of experiments (WT and misexpression) that can be reproduced at a single point in parameter space. *The numbers in white* are the Pearson's correlation (r_p) and Spearman's correlation (r_s) of each metric with performance. The associated p values are computed using a two-tailed Student's t test for the Pearson's correlation and a permutation test for the Spearman's correlation. Many structure metrics have a significant but weak correlation with performance

the patterning of the forebrain of cichlid fish (Sylvester et al. 2010).

4.1 Free parameters

Although the differential equation model introduces several new parameters not present in the Boolean model, most of these were set to specific values intended to capture biological measurements. The only parameters that were free in the sense of being varied in order to optimise the fit between the model and the data were n and k. These were specific for each interaction, and generally, the networks we investigated (i.e. those identified as functional from the Boolean screen) had about 10 interactions (Giacomantonio and Goodhill, 2010).

Thus, there were about 20 free parameters we varied in each case. These parameters were varied to fit 12 experimental conditions (see Fig. 1), each of which required specific outcomes for all of the 5 genes and proteins. There were thus substantially more constraints than free parameters. Furthermore, unlike for instance adding higher-order terms to a polynomial curve fit, varying the precise form of each interaction via n and k does not necessarily improve the ability of the network to fit the data, since the primary constraint is the network structure itself.

4.2 Limitations of the model

Although we have presented the best performing network, we caution against interpreting this network as the most likely true network, since the model has a number of limitations. Firstly, as we have already discussed, the number of free parameters meant that our sampling of parameter space was limited, and there are likely many networks from the set we examined that can reproduce all current experimental data. It would be useful to show how our approach performs on synthetic data generated by a known network. As well as testing the robustness of the search functions, and pre-filtering, a synthetic data set would also help to address the question of what happens when only a subset of proteins are 'visible' to be fitted (see also below). Furthermore, there are likely additional networks that we did not examine that can also reproduce all current experimental data. Since ODE models can have additional steady states not found in the Boolean representation (Glass and Kauffman 1973; Wittmann et al. 2009b), there are some networks that we excluded based on the Boolean analysis that perform reasonably in the ODE model, as shown in our simulations of a random selection of these excluded networks (Fig. 6b). In addition, we only used sigmoidal Hill functions to describe transcriptional regulation and only combined the action of multiple regulators on a target mRNA multiplicatively, when other functions are possible (Schilstra and Nehaniv 2008). We also only explored a single choice of parameter changes to simulate the misexpression mice and did not explore whether it is necessary to explicitly model proteins. It is quite likely that this is not actually required. Nevertheless, the existence of functional networks additional to those we considered does not undermine our conclusion that many different configurations of networks of five genes are capable of reproducing the existing experimental data.

Our two compartment model cannot capture gradient formation or other more complex dynamics (such as those between *Fgf8*, *Emx2* and *Sp8* (Fukuchi-Shimogori and Grove 2003; Sahara et al. 2007; Zembrzycki et al. 2007)). However, at present, there are almost no data regarding mechanisms of communication between ends of the developing cortex, and a model that included molecular transport would necessarily be based on many additional assumptions. Exploring these issues in a model will become computationally feasible as additional spatial data becomes available to constrain parameter choices, or at least give a smaller space of possible networks. Due to the limitations inherent in representing gradients in ODE models, it may be advantageous in the future to move to a model that allows a more realistic representation, such as a partial differential equation model.

How can we be sure that there is not a missing protein that when included 'completes' the network? To address this, we performed a preliminary investigation of the effect on performance of adding a currently unidentified molecule to the network (data not shown). However, to do this investigation, we had to make so many choices unconstrained by data—Which base network should we start with? How does the latent factor regulate the base network? Is it regulated by the network? If not, what is its expression pattern?—that the results were not informative. Hence, explorations of this type, which have been performed for other networks (Albert and Othmer 2003; Dayarian et al. 2009; Nakajima et al. 2010), are not yet possible for the arealisation regulatory network until the true structure of the network is better understood. Regardless, the analysis in this paper shows that multiple networks formed by *Fgf8* and the four transcription factors are likely sufficient to generate the observed expression patterns in WT and misexpression mice.

4.3 The role of feedback

Experimental data indicate that the arealisation network contains many feedback loops, and our simulations confirm that many feedback-rich networks can reproduce the experimental data. This has several consequences on the types of questions about this network that can be answered. In such a highly connected network, most components cannot sensibly be considered to be upstream or downstream of each other. It may also be tautological to debate whether particular transcription factors induce posterior identity or suppress anterior identity (or vice versa) since, in a highly connected network, they can each perform both roles simultaneously. Instead, we suggest that a productive direction for the field could be to focus on determining what is downstream of the network as a whole, and understanding why the network is so highly connected. Experimental and theoretical work has demonstrated that different feedback motifs have specific purposes (Bolouri and Davidson 2002; Brandman and Meyer 2008; Davidson 2010), and once we elucidate the true structure of the arealisation network, we will be able to understand why various feedback motifs occur.

Having a feedback-rich network emphasises the fact that *Fgf8* cannot be said to be a morphogen in the strict sense of being a master pattern generator for a passive target tissue, which only interprets the gradient (Wolpert 1969). Instead,

in the telencephalon, the genes expressed in the target tissue appear to play an integral role, regulating *Fgf8* and shaping its expression pattern. Our modelling shows that a diversity of actions of the transcription factors on *Fgf8* could exist, and if this is true, a view of *Fgf8* as a master differentiating signal would hold only approximately. It is worth noting that the strictest definition of a morphogen has also been found to be too simplistic to be applied even to the archetypal morphogen, *Bicoid*, where the active role of the tissue it patterns has been demonstrated and emphasised (Jaeger et al. 2004; Jaeger and Reinitz 2006).

4.4 Suggested experiments to constrain the structure of the arealisation network

To date, research in this field has been largely driven by a debate on whether cortical arealisation was principally driven by genes or activity (Rakic 1988; O'Leary 1989). In accumulating evidence to answer this general question, experiments identified some of the key genes involved and established that the relevant gene regulatory network is rich in feedback (Mallamaci and Stoykova 2006; O'Leary et al. 2007; Rakic et al. 2009; Mallamaci 2011). Our work moves beyond a parts list and attempts to understand the true structure of this network using computational modelling. In other systems, an iterative cycle of modelling and wet laboratory experiments over many years has been useful in answering these types of questions (Thieffry and Sanchez 2003; Jaeger et al. 2004; Tomlin and Axelrod 2007), and our work represents one of the first attempts to initiate the use of this approach to understand cortical arealisation. Our analysis suggests that, precisely because the system appears to have so much feedback, the qualitative description of novel misexpression mice, and even the identification of new genes important to the network, will not allow us to uncover the true structure. Although our analysis did not allow us to make strong predictions about specific network structures, we suggest that this conclusion is an important point of consideration for future experiments in this field that aim to understand this regulatory network.

To continue to progress our understanding of cortical arealisation using a complementary modelling and experimental approach, we need some new directions in experiments. Any assays that confirm direct interactions or definitively eliminate possible interactions would be very useful from a modelling perspective because each additional possible interaction greatly increases the number of degrees of freedom in the model. To prioritise experiments, researchers could, for instance, use the predictions of more and less likely interactions listed in Giacomantonio and Goodhill (2010). As constraints are added, models can be refined, increasing their power to make specific predictions. By performing experiments and refining models in an iterative manner, there is potential for the true arealisation regulatory network to be uncovered efficiently.

Another avenue for experiments that could provide additional constraints is to fully characterise the expression of each of the genes of interest in each of the existing misexpression mice. To date, the expression of only a few of our five genes of interest has been described in each mouse, often in different sections. A description of each of these genes relative to WT levels in sagittal or serial coronal sections would be useful, more useful than incomplete descriptions of novel misexpression mice. Quantitative time courses of expression would be even more useful. Since numerical simulations produce complete time courses of expression (like Fig. 3c), comparison of these model outputs with similar quantitative data from mice could help distinguish between competing models. Alternatively, quantitative time courses of expression could enable attempts to reverse engineer the network (Yeung et al. 2002; Laubenbacher and Stigler 2004).

The Allen Institute's Developing Mouse Brain Atlas (2009) has characterised expression of many genes at several embryonic and early postnatal time points in WT mice, starting at E11.5. At present, this data set commences too late and is too coarse temporally to inform modelling of the arealisation regulatory network, but as the dataset grows it may become useful, particularly as it becomes more quantitative. While the decreasing cost of microarrays and RNAseq makes obtaining quantitative time series more achievable, the tissue samples would have to be on the order of 10^6 cubic microns to characterise spatial patterns, which presents challenges in dissection and analysis. To collect enough RNA to do a microarray analysis, Sansom et al. (2005) had to pool samples from multiple animals. Unfortunately, pooling samples are not ideal for the many arealisation misexpression mice created by *in utero* electroporation, as the level of gene expression cannot be calculated or repeated precisely.

5 Conclusions

Uncovering the true structure of this network may help us to answer the next question of how the gradients generated by this network dictate discrete area fates. A complementary programme of modelling and experiments may be the most efficient path to answering this question, as has occurred in the study of *Drosophila* embryonic development. Long before we have definitive answers though, modelling can be used to guide experiments by ranking alternative hypotheses and making predictions that distinguish between competing models (Kitano 2002; Fisher and Henzinger 2007). This paper introduces some of the methods used successfully in other systems to the field of arealisation. By showing that a diversity of networks can reproduce almost all the experimental data, we have demonstrated the need for new experiments

that identify direct interactions or quantify gene expression levels in order to continue to improve understanding of the genetic control of early arealisation.

Acknowledgments We thank Peter Dayan, Linda Richards, Guillermina López-Bendito, and the anonymous reviewers for their helpful feedback and comments on the manuscript. This work was supported by an Australian Postgraduate Award to CEG and the Human Frontier Science Program (Grant RPG0029/2008-C).

References

Albert R, Othmer HG (2003) The topology of the regulatory interactions predicts the expression pattern of the segment polarity genes in Drosophila melanogaster. J Theor Biol 223:1–18

Allen developing mouse brain atlas (2009) [Internet]. Seattle (WA): Allen Institute for Brain Science. http://developingmouse.brain-map.org

Armentano M, Chou SJ, Tomassy GS, Leingärtner A, O'Leary DDM, Studer M (2007) COUP-TFI regulates the balance of cortical patterning between frontal/motor and sensory areas. Nat Neurosci 10:1277–1286

Bolouri H, Davidson EH (2002) Modeling transcriptional regulatory networks. Bioessays 24:1118–1129

Brandman O, Meyer T (2008) Feedback loops shape cellular signals in space and time. Science 322:390–395

Chaves M, Sengupta A, Sontag E (2008) Geometry and topology of parameter space: investigating measures of robustness in regulatory networks. J Math Biol 59:315–358

Cholfin JA, Rubenstein JLR (2008) Frontal cortex subdivision patterning is coordinately regulated by Fgf8, Fgf17, and Emx2. J Comp Neurol 509:144–155

Davidson EH (2010) Emerging properties of animal gene regulatory networks. Nature 468:911–920

Dayarian A, Chaves M, Sontag ED, Sengupta AM (2009) Shape, size, and robustness: feasible regions in the parameter space of biochemical networks. PLoS Comput Biol 5:e1000256

De Jong H (2002) Modeling and simulation of genetic regulatory systems: a literature review. J Comput Biol 9:67–103

Fagiolo G (2007) Clustering in complex directed networks. Phys Rev E Stat Nonlin Soft Matter Phys 76:026107

Fisher J, Henzinger TA (2007) Executable cell biology. Nat Biotechnol 25:1239–1249

Fukuchi-Shimogori T, Grove EA (2003) Emx2 patterns the neocortex by regulating FGF positional signaling. Nat Neurosci 6:825–831

Garel S, Huffman KJ, Rubenstein JLR (2003) Molecular regionalization of the neocortex is disrupted in Fgf8 hypomorphic mutants. Development 130:1903–1914

Giacomantonio CE, Goodhill GJ (2010) A Boolean model of the gene regulatory network underlying mammalian cortical area development. PLoS Comput Biol 6:e1000936

Glass L, Kauffman SA (1973) The logical analysis of continuous, nonlinear biochemical control networks. J Theor Biol 39:103–129

Gleich D (2009) gaimc: graph algorithms in Matlab code. Accessed 12 Aug 2011. http://www.mathworks.com/matlabcentral/fileexchange/24134

Gorski JA, Talley T, Qiu M, Puelles L, Rubenstein JLR, Jones KR (2002) Cortical excitatory neurons and glia, but not GABAergic neurons, are produced in the Emx1-expressing lineage. J Neurosci 22:6309–6314

Grove EA, Fukuchi-Shimogori T (2003) Generating the cerebral cortical area map. Annu Rev Neurosci 26:355–380

Hamasaki T, Leingärtner A, Ringstedt T, O'Leary DDM (2004) EMX2 regulates sizes and positioning of the primary sensory and motor areas in neocortex by direct specification of cortical progenitors. Neuron 43:359–372

Hébert JM, Fishell G (2008) The genetics of early telencephalon patterning: some assembly required. Nat Rev Neurosci 9:678-685

Hébert JM, McConnell SK (2000) Targeting of cre to the Foxg1 (BF-1) locus mediates loxP recombination in the telencephalon and other developing head structures. Dev Biol 222:296–306

Holland J (1975) Adaptation in natural and artificial systems. University of Michigan Press, Ann Arbor, MI

Jaeger J, Reinitz J (2006) On the dynamic nature of positional information. Bioessays 28:1102–1111

Jaeger J, Surkova S, Blagov M, Janssens H, Kosman D, Kozlov KN, Vanario-Alonso CE, Samsonova M, Sharp DH, Reinitz J (2004) Dynamic control of positional information in the early Drosophila embryo. Nature 430:368–371

Job C, Tan SS (2003) Constructing the mammalian neocortex: the role of intrinsic factors. Dev Biol 257:221–232

Karbowski J, Ermentrout GB (2004) Model of the early development of thalamo-cortical connections and area patterning via signaling molecules. J Comput Neurosci 17:347–363

Kirkpatrick S, Gelatt CD, Vecchi MP (1983) Optimization by simulated annealing. Science 220:671–680

Kitano H (2002) Systems biology: a brief overview. Science 295:1662–1664

Laubenbacher R, Stigler B (2004) A computational algebra approach to the reverse engineering of gene regulatory networks. J Theor Biol 229:523–537

Mallamaci A (2011) Molecular bases of cortico-cerebral regionalization. Prog Brain Res 189:37–64

Mallamaci A, Stoykova A (2006) Gene networks controlling early cerebral cortex arealization. Eur J Neurosci 23:847–856

Meir E, Von Dassow G, Munro E, Odell GM (2002) Robustness, flexibility, and the role of lateral inhibition in the neurogenic network. Curr Biol 12:778–786

Meyers EN, Lewandoski M, Martin GR (1998) An Fgf8 mutant allelic series generated by Cre- and Flp-mediated recombination. Nat Genet 18:136–141

Muzio L, DiBenedetto B, Stoykova A, Boncinelli E, Gruss P, Mallamaci A (2002) Emx2 and Pax6 control regionalization of the preneuronogenic cortical primordium. Cereb Cortex 12:129–139

Nakajima A, Isshiki T, Kaneko K, Ishihara S (2010) Robustness under functional constraint: the genetic network for temporal expression in Drosophila neurogenesis. PLoS Comput Biol 6:e1000760

O'Leary DD (1989) Do cortical areas emerge from a protocortex? Trends Neurosci 12:400–406

O'Leary DD, Sahara S (2008) Genetic regulation of arealization of the neocortex. Curr Opin Neurobiol 18:90–100

O'Leary DDM, Chou SJ, Sahara S (2007) Area patterning of the mammalian cortex. Neuron 56:252–269

Pellegrini M, Mansouri A, Simeone A, Boncinelli E, Gruss P (1996) Dentate gyrus formation requires Emx2. Development 122:3893–3898

Rakic P (1988) Specification of cerebral cortical areas. Science 241:170–176

Rakic P, Ayoub AE, Breunig JJ, Dominguez MH (2009) Decision by division: making cortical maps. Trends Neurosci 5:291-301

Sahara S, Kawakami Y, Belmonte JCI, O'Leary DDM (2007) Sp8 exhibits reciprocal induction with Fgf8 but has an opposing effect on anterior-posterior cortical area patterning. Neural Dev 2:10

Sansom SN, Hébert JM, Thammongkol U, Smith J, Nisbet G, Surani MA, McConnell SK, Livesey FJ (2005) Genomic characterisation of a Fgf-regulated gradient-based neocortical protomap. Development 132:3947–3961

Schilstra MJ, Nehaniv CL (2008) Bio-logic: gene expression and the laws of combinatorial logic. Artif Life 14:121–133

Storm EE, Rubenstein JLR, Martin GR (2003) Dosage of Fgf8 determines whether cell survival is positively or negatively regulated in the developing forebrain. Proc Natl Acad Sci USA 100:1757–1762

Storm EE, Garel S, Borello U, Hebert JM, Martinez S, McConnell SK, Martin GR, Rubenstein JLR (2006) Dose-dependent functions of Fgf8 in regulating telencephalic patterning centers. Development 133:1831–1844

Sur M, Leamey CA (2001) Development and plasticity of cortical areas and networks. Nat Rev Neurosci 2:251–262

Sur M, Rubenstein JLR (2005) Patterning and plasticity of the cerebral cortex. Science 310:805–810

Sylvester JB, Rich CA, Loh YHE, van Staaden MJ, Fraser GJ, Streelman JT (2010) Brain diversity evolves via differences in patterning. Proc Natl Acad Sci USA 107:9718–9723

Thieffry D, Sanchez L (2003) Dynamical modelling of pattern formation during embryonic development. Curr Opin Genet Dev 13:326–330

Tomlin CJ, Axelrod JD (2007) Biology by numbers: mathematical modelling in developmental biology. Nat Rev Genet 8:331–340

Toyoda R, Assimacopoulos S, Wilcoxon J, Taylor A, Feldman P, Suzuki-Hirano A, Shimogori T, Grove EA (2010) FGF8 acts as a classic diffusible morphogen to pattern the neocortex. Development 137:3439–3448

Vanier MC, Bower JM (1999) A comparative survey of automated parameter-search methods for compartmental neural models. J Comput Neurosci 7:149–171

Von Dassow G, Meir E, Munro EM, Odell GM (2000) The segment polarity network is a robust developmental module. Nature 406:188–192

Wittmann DM, Blöchl F, Trümbach D, Wurst W, Prakash N, Theis FJ (2009a) Spatial analysis of expression patterns predicts genetic interactions at the mid-hindbrain boundary. PLoS Comput Biol 5:e1000569

Wittmann DM, Krumsiek J, Saez-Rodriguez J, Lauffenburger DA, Klamt S, Theis FJ (2009b) Transforming Boolean models to continuous models: methodology and application to T-cell receptor signaling. BMC Syst Biol 3:98

Wolpert L (1969) Positional information and the spatial pattern of cellular differentiation. J Theor Biol 25:1–47

Yeung MKS, Tegnér J, Collins JJ (2002) Reverse engineering gene networks using singular value decomposition and robust regression. Proc Natl Acad Sci USA 99:6163–6168

Zembrzycki A, Griesel G, Stoykova A, Mansouri A (2007) Genetic interplay between the transcription factors Sp8 and Emx2 in the patterning of the forebrain. Neural Dev 2:8